Supporting Information

Hydrogen-free exsolution of Ir-Fe nanoalloys on solid oxide cell perovskite air electrode surface

Jiyoon Shin[a,b†], Myung-Jin Jung[c†], Hao-Yang Li[b], Yujie Wu[a], Wanwisa Limphirat[d], Se-Hun Kwon[c*], Pei-Chen Su[a,b*]

[a] School of Mechanical and Aerospace Engineering, Nanyang Technological University 50 Nanyang Avenue, 639798, Singapore

[b] Energy Research Institute @ NTU (ERI@N), Interdisciplinary Graduate School, Nanyang Technological University, 50 Nanyang Drive, Singapore, 637553, Singapore

[c] School of Materials Science and Engineering, Pusan National University, Busan 46241, Republic of Korea

[d] Synchrotron Light Research Institute (Public Organization), 111 University Avenue, Muang District, Nakhon Ratchasima 30000, Thailand

[*] Email addresses: sehun@pusan.ac.kr (S.-H. Kwon).

[*] Email addresses: peichensu@ntu.edu.sg (P.-C. Su).

[†] J. Shin and M.-J. Jung contributed equally to this work

Experimental Section

SFMO Electrode Fabrication: $Sr_2Fe_{1.5}Mo_{0.5}O_{6-\delta}$ (SFMO) powder was synthesized via a glycine-nitrate combustion process. Stoichiometric amounts of $Sr(NO_3)_2$ (Sigma-Aldrich, ≥ 99.95 %), $Fe(NO_3)_3 \cdot 9H_2O$ (Sigma-Aldrich, ≥ 99.95 %), $(NH_4)_6Mo_7O_{24} \cdot 4H_2O$ (Sigma-Aldrich, ≥ 99.98 %) were dissolved in deionized water with glycine and citric acid as complexing agents. The solution was stirred overnight, adjusted to pH 8 with NH_4OH (Merck, 25 %), and heated at 80 ˚C to form a gel. The gel was combusted at 250 ˚C, and the resulting ash was calcined at 1100 ˚C for 5 hours in air to obtain the final SFMO powder. Dense $La_{0.8}Sr_{0.2}Ga_{0.8}Mg_{0.2}O_{3-\delta}$ (LSGM) electrolyte pellets (11 mm diameter, 0.3 mm thickness) were prepared by uniaxial pressing of commercial LSGM powder (Fuel Cell Materials, USA) and sintering in air at 1450 ˚C for 5 hours. The SFMO powder was mixed with VEH binder (Fuel Cell Materials, USA) to form an ink, which was screen-printed onto the LSGM pellets and sintered at 1000 ˚C for 5 hours to form porous electrodes.

ALD Ir coating: Uniform Ir nanoparticles were deposited on the SFMO electrodes using a Lucida D-100 ALD system (NCD). The desired nanoparticle density was achieved with 50 ALD cycles, based on the measured growth-per-cycle (GPC) of the process. Prior to deposition, all cells were loaded into the ALD chamber and held at the target growth temperature for 30 min to ensure complete thermal equilibration. Tricarbonyl (1,2,3-η)-1,2,3-tri(*tert*-butyl)-cyclopropenyl iridium ($C_{18}H_{27}IrO_3$ or TICP) and oxygen (O_2) gas were employed as the Ir precursor and reactant, respectively. The precursor canister is maintained at 70 ˚C (TICP) to secure sufficient vapor pressure. Throughout the ALD process, the chamber pressure was stabilized at ~ 1 Torr under a continuous N_2 carrier gas flow. Each ALD cycle consisted of a 20 s TICP pulse followed by a 20 s N_2 purge with 100 sccm, and a subsequent 15 s O_2 pulse followed by a 20 s N_2 purge. This Ir decorated SFMO was deposited at growth temperatures of 250 ˚C.

Material Characterizations: The morphology and elemental composition of the electrodes were characterized by high-resolution transmission electron microscopy (HRTEM), high-angle annular dark-field scanning transmission electron microscopy (HAADF-STEM) coupled with energy-dispersive X-ray spectroscopy (EDX). General TEM/STEM imaging and EDX analyses were performed using a JEOL JEM-2100F-A microscope operated at 200 kV. For EDX mapping on the JEM-2100F-A, a Be double-tilt holder was used to improve X-ray collection and minimize holder-related shadowing during elemental analysis. High-resolution STEM imaging and STEM-EDX mapping of representative Ir-containing nanoparticles after air annealing, including the regions shown in **Figure 2c-d** and **Figure S3**, were further performed using a probe aberration-corrected JEOL JEM-ARM200F operated at 200 kV. Surface chemistry was analyzed by X-ray photoelectron spectroscopy (XPS) on a Shimadzu Kratos Axis Supra system, with spectra collected after gentle Ar^+ etching to remove surface carbon contaminants. The C 1s peak at 284.8 eV was used for binding energy calibration. Ex-situ Fe K-edge and Ir L_3-edge X-ray absorption spectroscopy (XAS) was conducted at Beamline 5.2 of the Synchrotron Light Research Institute (SLRI), Thailand, in a flow of synthetic air (8 sccm O_2 mixed with 32 sccm N_2 flow). Spectra were collected at room temperature, before and after annealing at 800 ˚C. Data processing was performed using the Athena software package.[1]

Electrochemical Characterizations: Electrochemical impedance spectroscopy (EIS) was performed on a half-cell configuration using a Biologic VP-300 potentiostat. The SFMO electrode served as the working electrode, with Ag paste (Fuel Cell Materials, USA) applied as the counter and reference electrodes. Measurements were conducted under open-circuit voltage in ambient air at 800 ˚C, over a frequency range of 1 MHz to 0.01 Hz with a 10 mV AC amplitude. The distribution of relaxation time (DRT) analysis was applied to deconvolute the electrochemical

processes using dedicated DRTtools software.[2] The test temperature of 800 ˚C was selected because it lies within the commonly used 750 – 850 ˚C operating window for SFMO-based air electrodes, while prior studies on perovskite exsolution and cation diffusion indicate that cation redistribution becomes kinetically accessible in this high-temperature regime.[3-6] Accordingly, the proposed pathway is described here as a qualitative kinetic picture involving thermally activated Fe redistribution, interfacial capture by Ir-rich particles, and formation of Ir–Fe alloy-like coordination, rather than as a fully quantified elementary-step kinetic model.[7-9]

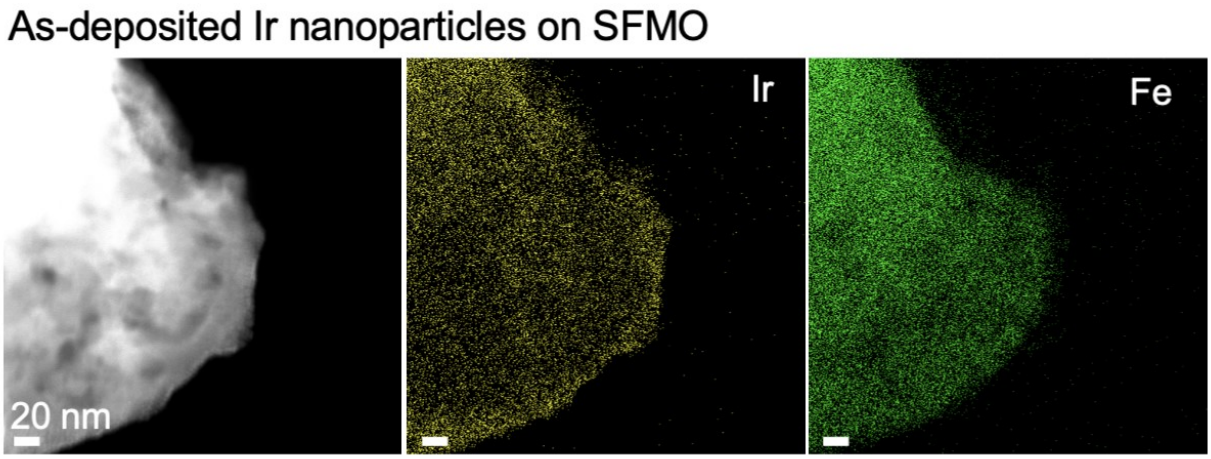

Figure S1. STEM-EDX mapping of as-deposited Ir nanoparticles on SFMO before air annealing. HAADF-STEM image and corresponding elemental maps of Ir and Fe show that ALD-deposited Ir nanoparticles are distributed on the SFMO surface before thermal treatment, while Fe remains primarily associated with the SFMO matrix. This initial state is compared with the annealed Ir/SFMO sample in **Figure 2** and **Figure S2**, where local Ir–Fe co-enrichment is observed within socketed nanoparticles after 800 ˚C air annealing.

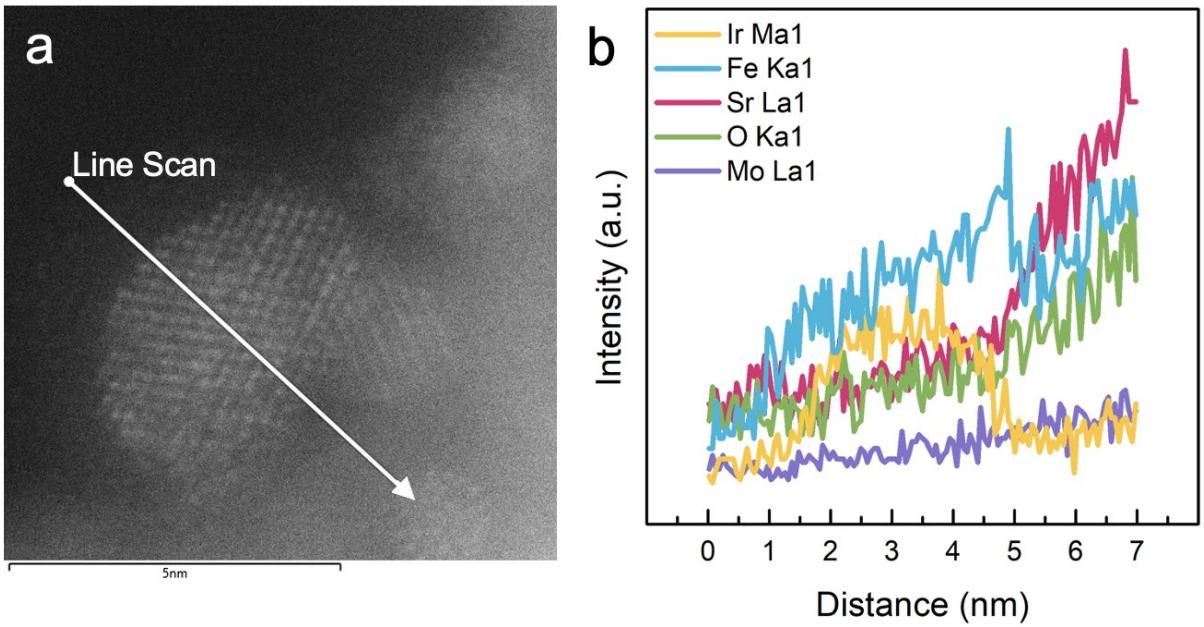

Figure S2. EDX line-scan analysis corresponding to the socketed Ir-containing nanoparticle after 800 ˚C air annealing for 50 h, shown in **Figure 2c-d**. (a) High-magnification STEM image showing the line-scan path across the nanoparticle/SFMO interface region. (b) Corresponding EDX line-scan profiles of Ir, Fe, Sr, O, and Mo. The Ir signal is locally enhanced within the nanoparticle region and is accompanied by Fe enrichment, while Sr, O, and Mo primarily increase toward the surrounding SFMO matrix. These data provide line-scan support for local Fe enrichment within the Ir-containing socketed nanoparticle region observed in **Figure 2c-d**.

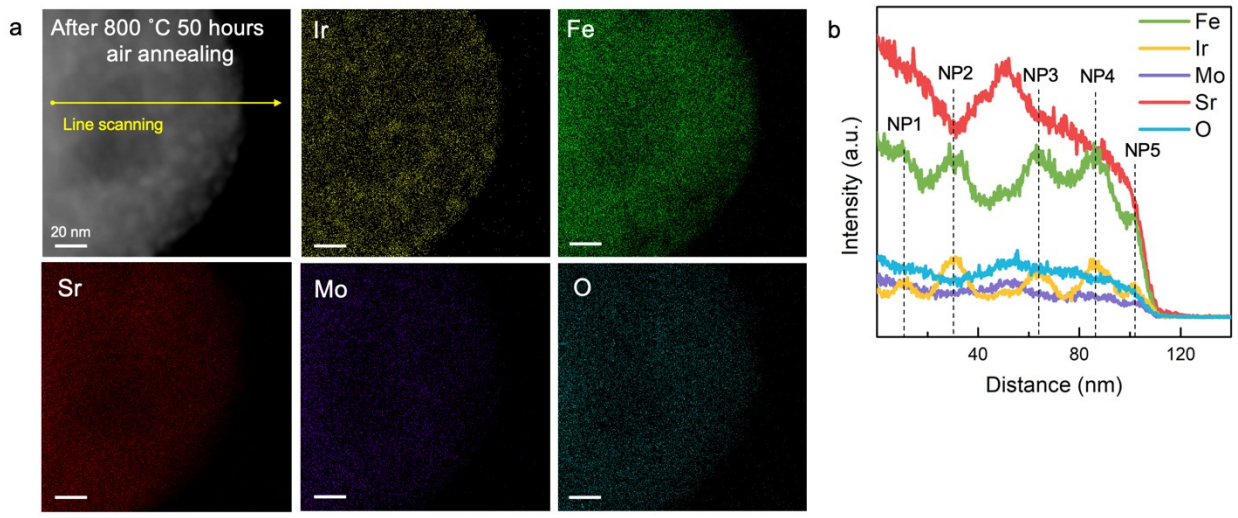

Figure S3. STEM-EDX mapping and line-scan analysis of Ir-decorated SFMO after 800 ˚C air annealing for 50 h. (a) HAADF-STEM image and elemental maps of Ir, Fe, Sr, Mo, and O around Ir-containing nanoparticles. The dashed marks are nanoparticles of NP1-NP5. (b) EDX line-scan profiles across the Ir−Fe nanoparticle/SFMO region. The Ir signal is locally enhanced at NP1-NP5, accompanied by Fe signal enhancement at the same nanoparticle positions, while Sr, Mo, and O primarily follow the SFMO matrix. These results support local Fe redistribution into Ir-containing nanoparticles.

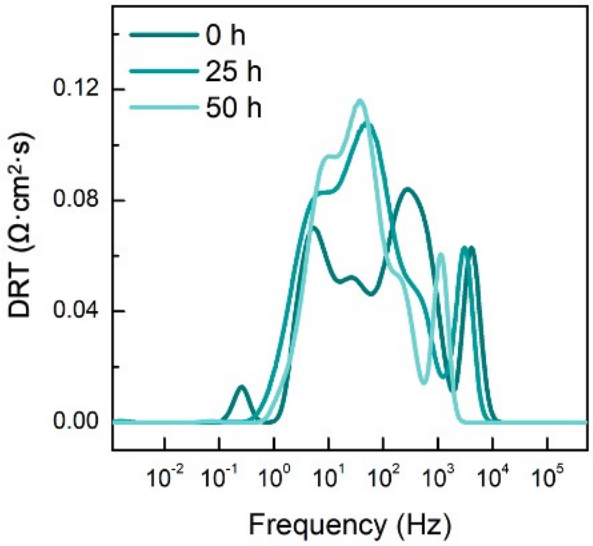

Figure S4. Distribution of relaxation times (DRT) evolution over time (0 h, 25 h, 50 h) for the Ir-Fe/SFMO electrode at 800 ˚C in air.

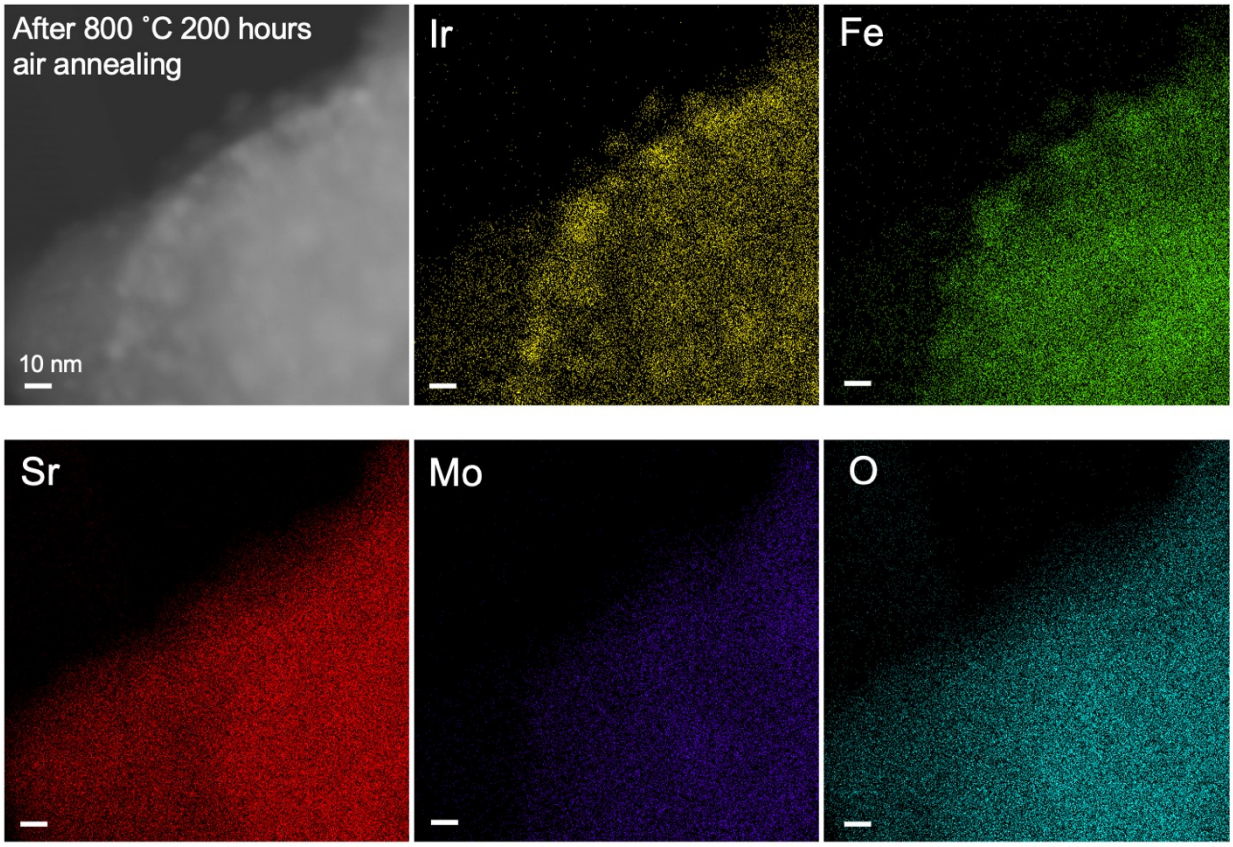

Figure S5. STEM-EDX mapping of Ir-decorated SFMO after prolonged air annealing at 800 °C for 200 h. HAADF-STEM image and corresponding elemental maps of Ir, Fe, Sr, Mo, and O show that Ir-containing nanoparticles remain associated with the SFMO surface after prolonged high-temperature oxidizing treatment. Ir and Fe remain spatially co-enriched in the nanoparticle regions, while Sr, Mo, and O primarily follow the surrounding SFMO matrix. These results provide additional microstructural evidence for the thermal persistence of Ir–Fe-containing nanoparticles under prolonged air annealing.

Reference

(1) Ravel, B.; Newville, M. ATHENA, ARTEMIS, HEPHAESTUS: data analysis for X-ray absorption spectroscopy using IFEFFIT. *Synchrotron Radiation* **2005**, *12* (4), 537-541.

(2) Wan, T. H.; Saccoccio, M.; Chen, C.; Ciucci, F. Influence of the discretization methods on the distribution of relaxation times deconvolution: implementing radial basis functions with DRTtools. *Electrochimica Acta* **2015**, *184*, 483-499.

(3) Bonkowski, A.; Wolf, M. J.; Wu, J.; Parker, S. C.; Klein, A.; De Souza, R. A. A single model for the thermodynamics and kinetics of metal exsolution from perovskite oxides. *Journal of the American Chemical Society* **2024**, *146* (33), 23012-23021.

(4) Calì, E.; Thomas, M. P.; Vasudevan, R.; Wu, J.; Gavalda-Diaz, O.; Marquardt, K.; Saiz, E.; Neagu, D.; Unocic, R. R.; Parker, S. C. Real-time insight into the multistage mechanism of nanoparticle exsolution from a perovskite host surface. *Nature communications* **2023**, *14* (1), 1754.

(5) Weber, M. L.; Šmíd, B.; Breuer, U.; Rose, M.-A.; Menzler, N. H.; Dittmann, R.; Waser, R.; Guillon, O.; Gunkel, F.; Lenser, C. Space charge governs the kinetics of metal exsolution. *Nature Materials* **2024**, *23* (3), 406-413.

(6) Kwon, O.; Sengodan, S.; Kim, K.; Kim, G.; Jeong, H. Y.; Shin, J.; Ju, Y.-W.; Han, J. W.; Kim, G. Exsolution trends and co-segregation aspects of self-grown catalyst nanoparticles in perovskites. *Nature communications* **2017**, *8* (1), 15967.

(7) Kubicek, M.; Rupp, G. M.; Huber, S.; Penn, A.; Opitz, A. K.; Bernardi, J.; Stöger-Pollach, M.; Hutter, H.; Fleig, J. Cation diffusion in La 0.6 Sr 0.4 CoO 3− δ below 800 C and its relevance for Sr segregation. *Physical Chemistry Chemical Physics* **2014**, *16* (6), 2715-2726.

(8) Qiu, P.; Lin, J.; Lei, L.; Yuan, Z.; Jia, L.; Li, J.; Chen, F. Evaluation of Cr-tolerance of the Sr2Fe1. 5Mo0. 5O6− δ cathode for solid oxide fuel cells. *ACS Applied Energy Materials* **2019**, *2* (10), 7619-7627.

(9) Xiao, G.; Liu, Q.; Zhao, F.; Zhang, L.; Xia, C.; Chen, F. Sr2Fe1. 5Mo0. 5O6 as cathodes for intermediate-temperature solid oxide fuel cells with La0. 8Sr0. 2Ga0. 87Mg0. 13O3 electrolyte. *Journal of The Electrochemical Society* **2011**, *158* (5), B455-B460.